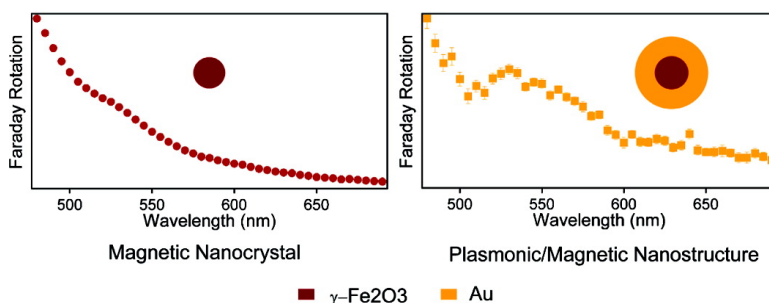


Surface Plasmon Resonance Enhanced Magneto-Optics (SuPREMO): Faraday Rotation Enhancement in Gold-Coated Iron Oxide Nanocrystals

Prashant K. Jain, Yanhong Xiao, Ronald Walsworth, and Adam E. Cohen

Nano Lett., Article ASAP • DOI: 10.1021/nl900007k • Publication Date (Web): 13 March 2009

Downloaded from <http://pubs.acs.org> on March 14, 2009



More About This Article

Additional resources and features associated with this article are available within the HTML version:

- Supporting Information
- Access to high resolution figures
- Links to articles and content related to this article
- Copyright permission to reproduce figures and/or text from this article

[View the Full Text HTML](#)

Surface Plasmon Resonance Enhanced Magneto-Optics (SuPREMO): Faraday Rotation Enhancement in Gold-Coated Iron Oxide Nanocrystals

Prashant K. Jain,[†] Yanhong Xiao,[‡] Ronald Walsworth,^{‡,§} and Adam E. Cohen^{*,†,§}

Department of Chemistry and Chemical Biology, Department of Physics, Harvard University, Cambridge, Massachusetts, 02138, and Harvard-Smithsonian Center for Astrophysics, Cambridge, Massachusetts, 02138

Received January 1, 2009; Revised Manuscript Received March 2, 2009

ABSTRACT

We report enhanced optical Faraday rotation in gold-coated maghemite (γ -Fe₂O₃) nanoparticles. The Faraday rotation spectrum measured from 480–690 nm shows a peak at about 530 nm, not present in either uncoated maghemite nanoparticles or solid gold nanoparticles. This peak corresponds to an intrinsic electronic transition in the maghemite nanoparticles and is consistent with a near-field enhancement of Faraday rotation resulting from the spectral overlap of the surface plasmon resonance in the gold with the electronic transition in maghemite. This demonstration of surface plasmon resonance-enhanced magneto-optics (SuPREMO) in a composite magnetic/plasmonic nanosystem may enable design of nanostructures for remote sensing and imaging of magnetic fields and for miniaturized magneto-optical devices.

Nanostructures of noble metals, especially gold (Au), silver (Ag), and copper (Cu), are interesting from both fundamental and technological standpoints due to their localized surface plasmon resonance, which is the collective oscillation of the conduction electrons when excited with visible light.^{1,2} Plasmon resonances impart these nanostructures with unusual optical properties, such as strongly enhanced size-, shape-, and medium-dependent light absorption and Mie scattering.^{2–5} Localized surface plasmons have been employed in a wide range of applications⁶ including imaging,^{7,8} chemical and biological sensing and probing,^{9–11} and targeted photothermal therapy.^{8,12,13} In addition to these far-field optical attributes, excitation of localized surface plasmon resonances results in strong confinement of electric fields around the nanostructure,^{14–16} causing near-field enhancements of linear and nonlinear optical processes.^{17,18} A prime example of such electromagnetic field enhancement is the amplification of Raman scattering by 10^5 – 10^6 for molecules adsorbed on gold or silver nanoparticles¹⁹ (and up to 10^{14} – 10^{15} at “hot spots” at the intersection of two or more nanoparticles^{20,21}). In recent years, plasmonic enhancement of photoluminescence from fluorophores,^{22–24} infrared vibrational absorption,¹⁷ second

harmonic processes,^{25–27} and photochemistry²⁸ have also been demonstrated using metal nanostructures.

The rotation of the polarization of light in a magnetized medium can be observed either in reflection (Kerr rotation) or in transmission (Faraday rotation).²⁹ Magneto-optical (MO) phenomena provide physical information on electronic and spin structure of materials^{30–32} and have also found applications in magnetic field sensors, optical isolators, data storage, and fast optical modulation.²⁹ Here, we demonstrate a new surface plasmon enhanced MO effect, which we call “SuPREMO”, in the form of enhanced optical Faraday rotation in a composite nanostructure consisting of magnetic maghemite nanoparticles coated with a plasmonic gold shell.

MO effects in most media are typically small. One approach for enhancing MO effects is the integration of MO-active media with photonic crystals, leading to enhanced Faraday rotation at the photonic band gap edge.^{33,34} Another theoretical proposal involves the use of metal films with arrays of subwavelength holes filled with an MO-active material.^{35,36} These structures support electromagnetic modes displaying extraordinary optical transmission (EOT) along with high Faraday rotation.

There has been recent interest in employing optical resonances of noble metal nanostructures for enhancing MO phenomena.^{37–45} Hui and Stroud proposed on theoretical grounds that media containing noble metal nanoparticles should show enhanced Faraday rotation at optical frequencies

* To whom correspondence should be addressed. E-mail: cohen@chemistry.harvard.edu.

[†] Department of Chemistry and Chemical Biology, Harvard University.

[‡] Harvard-Smithsonian Center for Astrophysics.

[§] Department of Physics, Harvard University.

corresponding to the localized surface plasmon resonance.⁴⁰ Early studies on Fe/Cu bilayer films showed an enhanced Kerr rotation response in the spectral region corresponding to the metal bulk plasmon edge.^{46,47} Multilayered ferromagnetic/noble metal structures,^{48–50} especially the Au/Co/Au system,³⁷ have been observed to exhibit Kerr rotation enhancement due to the thin-film surface plasmon resonance of the noble metal. Recent experiments have shown that magnetic films integrated with gold nanoparticles show enhanced Kerr rotation at the localized surface plasmon resonance of the gold nanoparticles.^{37–39}

One can classify enhancement in composite magnetic/plasmonic systems into two categories, depending on the relative positions of plasmonic and MO resonances and the measurement wavelength. When the plasmon resonance is far from any MO resonances, the MO enhancement is expected to occur with the same spectral dependence as the plasmon resonance.^{37–39} When there is good overlap between the plasmonic and the MO resonances, a plasmon resonance can cause an enhancement in a MO resonance of the nearby nonplasmonic magnetic medium. The MO enhancement in this case reflects the spectrum of electronic transitions of the nonplasmonic magnetic medium. The studies mentioned above demonstrate the first type of enhancement, but there has not been a clear demonstration of the latter form of enhancement arising from the overlap of a plasmonic and a MO resonance. A recent paper by Tomita et al. suggested such an enhancement in the Kerr rotation in a yttrium–iron garnet thin film incorporated with gold nanoparticles, but the effect was not well resolved.⁴² Li et al. studied the Faraday rotation of pairs of CoFe₂O₄ and Ag nanoparticles at a few discrete wavelengths and found differences from the Faraday rotation of CoFe₂O₄ nanoparticles, but the lack of full spectra leaves the interpretation of the nature of the plasmonic effect ambiguous.⁴⁵ The SUPREMO effect demonstrated here is the first example of a nanostructure composite of a magneto-optically active material and a plasmonic metal showing plasmon-enhanced MO effects. As described below, we observe enhanced visible-region Faraday rotation for gold-coated maghemite (γ -Fe₂O₃) nanoparticles at wavelengths \sim 530 nm, where there is spectral overlap of the surface plasmon resonance in gold with an intrinsic electronic transition in maghemite. In contrast, we observe no enhanced Faraday rotation for either uncoated maghemite nanoparticles or solid gold nanoparticles. These observations are consistent with localized surface plasmons excited in the nanostructure enhancing the MO effect of the electronic transition in γ -Fe₂O₃ nanoparticles.

Composite magnetic/plasmonic nanostructures were fabricated using a colloidal method.⁵¹ First, Fe₃O₄ (magnetite) nanoparticles were synthesized by the coprecipitation of Fe(II) and Fe(III) chlorides with NaOH as the reducing agent. A 25 mL solution containing 10 mmol FeCl₂·4H₂O and 20 mmol FeCl₃·6H₂O with 10 mmol HCl was added dropwise to a 250 mL solution of 1.5 M NaOH under vigorous stirring, resulting in the formation of a black precipitate (Fe₃O₄ nanoparticles). The precipitate was washed with Nanopure water followed by washing with 0.1 M HNO₃ solution and

centrifugation at 6000 rpm for 20 min. The precipitate was redispersed in 0.03 M HNO₃ solution and heated in a water bath at 90–100 °C for at least 30 min., resulting in the complete oxidation of the Fe₃O₄ colloid to the reddish brown γ -Fe₂O₃ (maghemite) colloid. The γ -Fe₂O₃ colloid was centrifuged at 6000 rpm for 20 min and the precipitate was washed first with water and then with 0.1 M tetramethyl ammonium hydroxide (TMAOH) solution, followed by an additional centrifugation step at 6000 rpm for 20 min. The nanoparticles were redispersed in 0.1 M TMAOH solution. The hydroxide ions from TMAOH adsorb to the surface of the iron oxide nanoparticles forming a passivating double-layer. X-ray diffraction (XRD) measurements on a dried sample of the colloid confirmed the synthesis of γ -Fe₂O₃ (Scintag XDS 2000 diffractometer, copper-K radiation 1.5406 Å). The XRD pattern (Figure 1a) shows peaks corresponding to known lattice planes in maghemite. The lattice parameter estimated from the diffraction peaks (8.34 + 0.02 Å) agrees well with the literature value for maghemite.⁵²

Next, the maghemite nanoparticles were coated with gold by the iterative seeding method described previously.⁵¹ Typically 80 mL of a γ -Fe₂O₃ colloid solution (\sim 0.05 mM in γ -Fe₂O₃ units) was stirred vigorously with 5 mM sodium citrate for at least 10 min to replace the surface hydroxide ions with citrate ions, which serve as a stabilizing agent for the gold coating. To this solution, HAuCl₄ solution (1% by Au weight) was added followed by an equal volume of 0.2 M hydroxylamine hydrochloride (NH₂OH·HCl). Four iterations of these additions were performed with at least 10 min between subsequent additions. The hydroxylamine hydrochloride reduces the Au³⁺ to Au, but does so preferentially on the surface of the citrate-capped γ -Fe₂O₃ nanoparticles.⁵³ The gold nuclei initially formed on the γ -Fe₂O₃ surface act as seeds for further Au³⁺ reduction in subsequent iterations.

The formation of the gold coating on the γ -Fe₂O₃ was characterized by following the UV–visible extinction spectra on an Ocean Optics USB 4000 spectrometer (150 ms integration time, 100 averages, and boxcar width of 2). As shown in Figure 2, the extinction spectrum of the unmodified γ -Fe₂O₃ nanoparticles does not show any strong absorption in the visible region. Following the first deposition of gold, a visible absorption band develops at around 614 nm, which can be attributed to the localized surface plasmon resonance of the gold-coated nanostructure. It is well established that a nanostructure consisting of a gold shell around a dielectric core shows a plasmon resonance significantly red-shifted compared to the plasmon resonance of a solid gold nanosphere, which is known to be around 520 nm.^{54,55} This red shift is due to the electromagnetic coupling between the plasmon oscillations on the inner and the outer surfaces of the gold shell. With further addition of gold, we found that the plasmon resonance band shifts toward the blue and becomes narrower, consistent with an increase in the thickness of the gold coating. Other factors, such as a change to a more spherical shape and filling of the initial hollow shell may also contribute.⁵¹ The plasmon band did not blue shift much after the fifth iteration of gold addition. Thus,

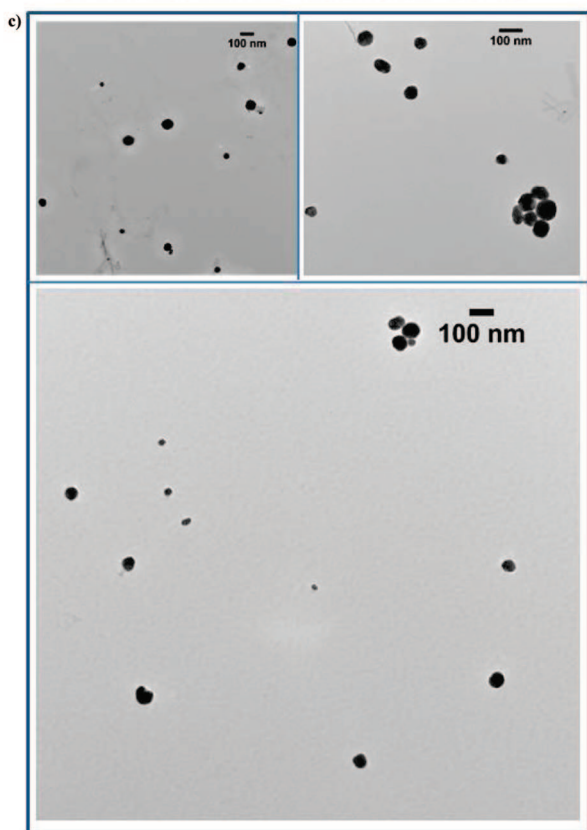
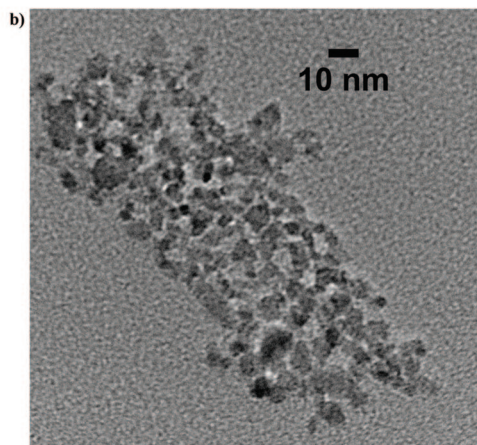
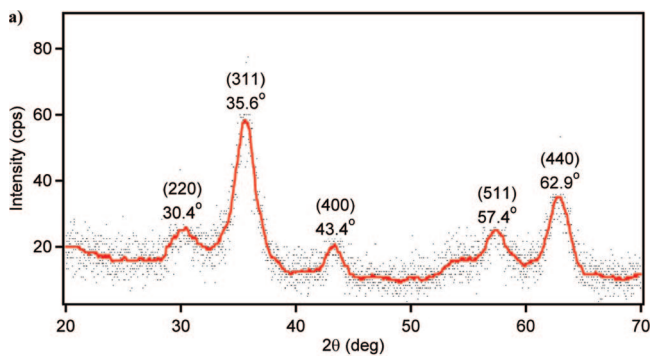


Figure 1. (a) Powder XRD pattern for γ - Fe_2O_3 nanoparticles. The red curve is a 50-point median averaging of the data. Five diffraction peaks have been assigned based on literature and used to calculate a lattice parameter of $8.34 \pm 0.02 \text{ \AA}$. Representative transmission electron microscopy images of (b) bare γ - Fe_2O_3 nanoparticles and (c) gold-coated γ - Fe_2O_3 nanoparticles following magnetic separation and purification steps.

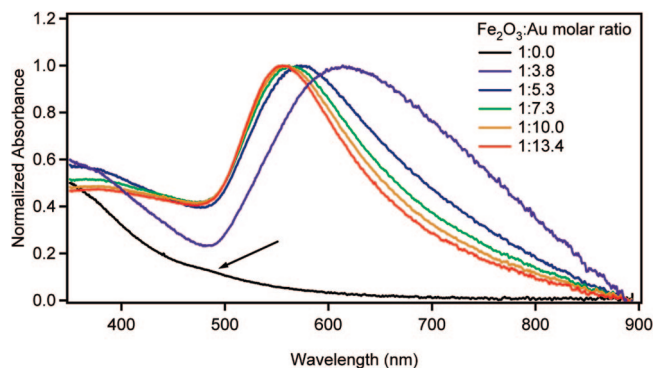


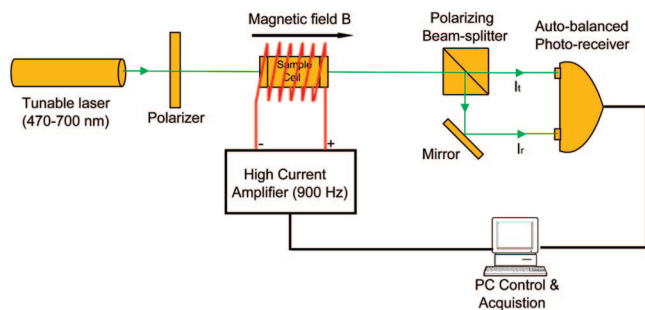
Figure 2. UV-visible absorbance spectra of gold-coated γ - Fe_2O_3 nanoparticles shown as a function of the molar ratio of the maghemite nanoparticles (in Fe_2O_3 units) to Au ions added during the iterative gold-coating process. The spectrum for bare γ - Fe_2O_3 nanoparticles is shown in black. The black arrow indicates the shoulder absorption corresponding to an electronic transition in γ - Fe_2O_3 .

we selected the fifth-iteration gold-coated γ - Fe_2O_3 nanoparticles for further characterization. The nanoparticles were subjected to separation on a strong neodymium magnet to isolate them from any purely gold particles that may have nucleated. The magnetically separated precipitate was then centrifuged at a low speed (800 rpm) for 20 min to remove any γ - Fe_2O_3 nanoparticles that may have remained uncoated. The latter purification steps are important to ensure that the samples consist predominantly of the composite plasmonic/magnetic nanostructures. Following the purification steps, the gold-coated γ - Fe_2O_3 nanoparticles showed a plasmon resonance band maximum at about 560 nm.

Transmission electron microscopy (TEM) images of both uncoated γ - Fe_2O_3 nanoparticles and the purified gold-coated nanoparticles (shown respectively in Figure 1b,c) were taken on a JEOL 2100 TEM operating at 200 kV. TEM samples were prepared by drop-casting $2 \mu\text{L}$ of the sonicated colloidal solution on a carbon-coated Formvar-supported 100 mesh copper grid and drying the solution in air. From a representative TEM image (Figure 1b), the uncoated γ - Fe_2O_3 nanoparticles showed an average diameter of 5.1 nm (with a 1.5 nm standard deviation). At this size, γ - Fe_2O_3 nanoparticles are superparamagnetic.⁵² The gold coating resulted in nanoparticles with an average diameter of 54.7 nm (with a standard deviation of 18.5 nm), and much higher electron microscopy contrast due to the gold.

Faraday rotation measurements of Fe_3O_4 , γ - Fe_2O_3 , pure gold, and gold-coated γ - Fe_2O_3 nanoparticles were performed in the visible spectral range. The optical setup (shown in Scheme 1) consisted of a supercontinuum fiber laser (Fianium, Inc.) with an acousto-optic tunable filter (Crystal Technology, Inc.), which allowed the tuning of the illumination wavelength λ from 480 to 690 nm. The laser beam was linearly polarized by passing through a Glan Thompson polarizer (extinction ratio 10^5) and then transmitted through the sample solution in a 1 cm path length optical cell placed in the core of a homemade electromagnet. The electromagnet was driven by a high-current amplifier at 900 Hz, generating a peak magnetic field of 150 Gauss. The beam transmitted

Scheme 1. Experimental Setup for Faraday Rotation Measurement



through the sample was then passed through a visible-range polarizing beamsplitter, which splits the beam of intensity I into a transmitted beam of intensity I_t and a reflected beam of intensity I_r . For a small clockwise Faraday rotation θ , we have

$$I_t = \frac{I}{2}(1 + \cos 2\varphi + 2\theta \sin 2\varphi) \quad (1)$$

$$I_r = \frac{I}{2}(1 - \cos 2\varphi - 2\theta \sin 2\varphi) \quad (2)$$

where φ is the angle between the input polarization from the laser and the horizontal axis of the polarizing beamsplitter. An autobalanced photodetector (New Focus Nirvana 2007) was employed to measure I_t and I_r . For proper function of the autobalancing circuit, φ was set to 54.7° , yielding $I_r \approx 2I_t$. The Faraday rotation angle θ was extracted by software lock-in at the magnetic field modulation frequency (900 Hz) and measured as a function of wavelength from 480 to 690 nm in 5 nm increments. Spectra were generated by typically averaging 10 such wavelength scans. Using this setup, we measured the Verdet constant of water to be $3.79 \pm 0.01 \times 10^{-6}$ rad/G·cm at 590 nm within <1% of the literature value of 3.80×10^{-6} rad/G·cm.⁵⁶ The Verdet constant for water was taken to have a positive sign as per literature convention.⁵⁷ The measured Faraday rotation of water was found to be a linear function of $1/\lambda^2$, typical of diamagnetic materials.

In Figure 3, the Faraday rotation spectra of γ -Fe₂O₃ nanoparticles, Fe₃O₄ nanoparticles, gold-coated γ -Fe₂O₃ nanoparticles, and a mixture of γ -Fe₂O₃ nanoparticles and gold nanospheres are presented. The Faraday rotation due to the water and quartz windows of the sample cell has been subtracted. All spectra are normalized to their values at 480 nm. The normalization constants are 17.77, 16.75, 0.78, and 7.71 mdeg for the γ -Fe₂O₃ nanoparticles, Fe₃O₄ nanoparticles, gold-coated γ -Fe₂O₃ nanoparticles, and the mixture, respectively. The strong light absorption of the gold-coated γ -Fe₂O₃ nanoparticles restricted us to using a low particle concentration, resulting in a smaller magnitude of Faraday rotation. Error bars represent the standard error of the mean of 50 measurements for the gold-coated γ -Fe₂O₃ nanoparticles and 10 measurements for other samples.

Figure 3a shows that there is marked difference in the Faraday rotation spectra of the nanoparticles of the two iron

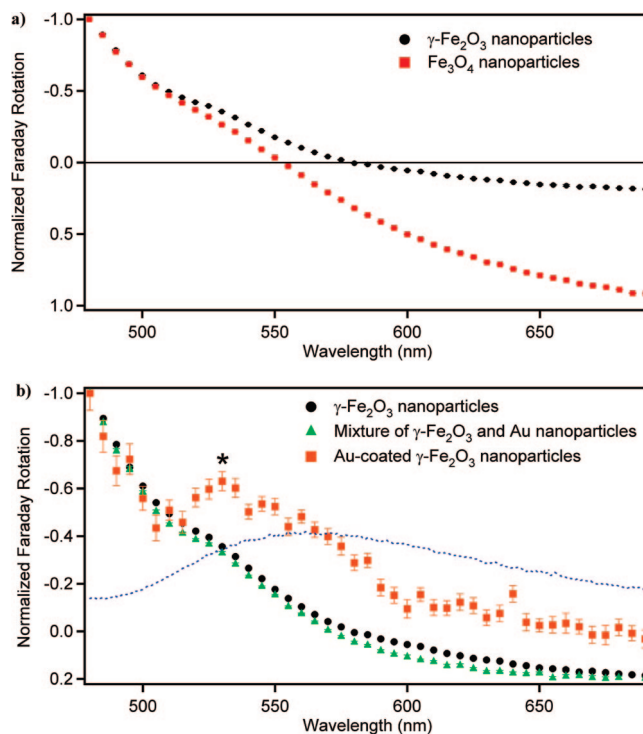


Figure 3. (a) Normalized Faraday rotation spectra of γ -Fe₂O₃ nanoparticles and Fe₃O₄ nanoparticles. (b) Normalized Faraday rotation spectra of γ -Fe₂O₃ nanoparticles, gold-coated γ -Fe₂O₃ nanoparticles, and a mixture of γ -Fe₂O₃ and gold nanospheres. The absorbance spectrum showing the plasmon resonance band of the gold-coated γ -Fe₂O₃ nanoparticles is indicated by the dotted blue curve. The * represents the position of the absorption band edge in γ -Fe₂O₃ determined from the photoluminescence spectrum in Figure 4.

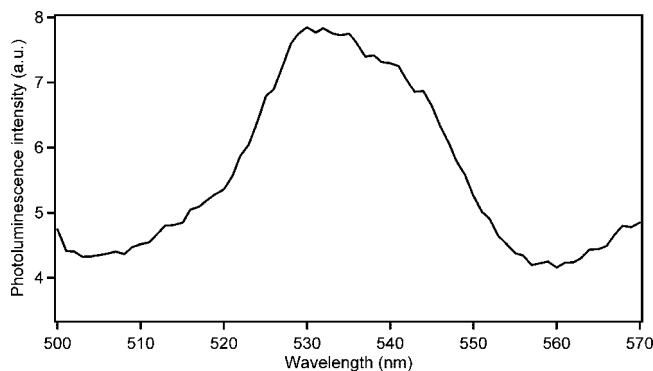


Figure 4. Photoluminescence spectrum of γ -Fe₂O₃ nanoparticles under 475 nm light excitation, showing an emission band at 530 nm.

oxides, Fe₃O₄ and γ -Fe₂O₃. Both oxides show a large negative Faraday rotation at 480 nm. This rotation is due to crystal field transitions in the 3d⁵ orbitals of Fe³⁺ (complicated by ligand-to-metal charge transfer interactions in the UV and blue region), which has been observed previously as a general feature of Fe³⁺-containing ferrite and garnet materials.^{30,32,58–60} In the case of the Fe₃O₄ nanoparticles, the Faraday rotation reaches zero near 555 nm and crosses over to a positive Faraday rotation, which further increases toward the near-infrared. The γ -Fe₂O₃ on the other hand

crosses zero at 580 nm and displays a relatively small positive Faraday rotation at longer wavelengths.

The comparatively large Faraday rotation of Fe₃O₄ nanoparticles as wavelengths approach the near-infrared is due to intervalence charge-transfer transitions (0.6 eV) between neighboring Fe³⁺ and Fe²⁺ ions in Fe₃O₄,⁶¹ which is a semimetal.⁶² γ -Fe₂O₃, on the other hand, has an optical absorption edge around 2 eV with only weak absorption in the near-infrared region.^{61,62} We note that the difference in the Faraday rotation spectra of Fe₃O₄ and γ -Fe₂O₃ nanoparticles could be used to quantitatively follow changes in the oxidation state of iron oxide. This information is typically accessible only by more sophisticated techniques such as X-ray absorption near-edge structure (XANES).^{62,63} In particular, we measured the ratio of Faraday rotation at 630 nm to that at 530 nm to be -0.34 for the γ -Fe₂O₃ nanoparticles, compared to -2.63 for the Fe₃O₄ nanoparticles.

The Faraday rotation spectra of uncoated and gold-coated γ -Fe₂O₃ nanoparticles are compared in Figure 3b. The gold-coated γ -Fe₂O₃ nanoparticles show an overall similar Faraday rotation spectrum to the uncoated particles, with the exception of a sharp peak that appears around 530 nm. The uncoated γ -Fe₂O₃ nanoparticles show only a weak shoulder in this region; no well-resolved resonant feature can be discerned. A simple “non-interacting” mixture of γ -Fe₂O₃ nanoparticles and colloidal gold nanospheres (green curve in Figure 3b) with an absorbance matched to that of the gold-coated γ -Fe₂O₃ nanoparticle sample also does not show the sharp Faraday rotation peak at 530 nm. This demonstrates that the rotation peak is not due merely to the presence of the gold component, but rather is a consequence of the close proximity of the gold and the γ -Fe₂O₃ in the composite γ -Fe₂O₃/gold nanostructure.

The Faraday rotation peak, observed at 530 nm for gold-coated γ -Fe₂O₃ nanoparticles, is blue shifted and much narrower compared to the gold plasmon absorption band, establishing that this enhanced Faraday rotation is not simply due to Faraday rotation associated with the plasmon resonance.^{38,39} As detailed below, we propose that localized surface plasmons excited in the nanostructure enhance the strength of a Faraday rotation band that is intrinsic to the γ -Fe₂O₃, but that is normally too weak to resolve.

On the basis of an estimated concentration of ~ 1.7 mM (in γ -Fe₂O₃ units) of the γ -Fe₂O₃ nanoparticles, we deduce a Faraday rotation at 480 nm of $-2.4^\circ \text{ T}^{-1}$ for a $\sim 1 \mu\text{m}$ path length of γ -Fe₂O₃ nanoparticles. The particle concentration for the gold-coated iron oxide nanoparticles is not known and therefore the rotation enhancement due to the addition of the gold shell cannot be directly estimated on a per-particle basis. However, by making a very rough approximation that the Faraday rotation at 480 nm is not affected by the plasmon resonance, we calculate an enhancement from the ratio of the rotation at 530 nm (normalized to the rotation at 480 nm) for the gold-coated particles to that of the uncoated particles. The enhancement factor estimated in this way is 1.75. The remarkable feature of the enhancement is the appearance of a sharp and previously indiscernible Faraday

rotation peak, rather than the numerical value of the enhancement over background.

The origin of the Faraday rotation peak at 530 nm can be traced to the electronic structure of the γ -Fe₂O₃, specifically the crystal field transitions of Fe³⁺ 3d⁵ electrons that dominate the visible spectrum of iron oxides.^{59,60} The crystal field transitions of the Fe³⁺ 3d electrons are in principle both spin- and parity-forbidden.⁶⁰ However, in ferrimagnets such as γ -Fe₂O₃, these transitions become weakly allowed^{32,60} due to the magnetic exchange coupling between Fe³⁺ centers (next-nearest neighbors) on antiparallel sublattices. Hence these transitions make a small contribution to the electronic absorption and magneto-optical activity.

γ -Fe₂O₃ has a weakly dipole-allowed electronic absorption in the 480–550 nm region, assigned by Sherman et al. to a “spin-flip” electron pair transition (EPT).^{60,64} The EPT involves the simultaneous excitation of two Fe³⁺ centers on neighboring antiparallel sublattices from their ground (⁶A₁) state to the first excited (⁴T₁) state, without a net change in spin.⁶⁰ In agreement with previous studies, the bare γ -Fe₂O₃ nanoparticles in the present study show a weak shoulder in the UV–vis absorption spectrum indicated by the black arrow in Figure 2. The band edge of this absorption band is obtained from a photoluminescence spectrum (Figure 4) of the γ -Fe₂O₃ nanoparticles (Varian Cary Eclipse spectrofluorimeter with a xenon lamp excitation source and 10 nm excitation and emission slits). Under 475 nm excitation, the γ -Fe₂O₃ nanoparticles show weak photoluminescence with a peak at 530 nm, corresponding to the band-edge emission of an electronic transition in γ -Fe₂O₃. A previous study on γ -Fe₂O₃ nanoparticles found a similar band edge and excitonic photoluminescence band around 520 nm.⁶⁵ The EPT, cited to be around 510 nm in γ -Fe₂O₃, is therefore the most likely assignment of this transition.⁶⁰ It is conceivable that the transition in the nanocrystals of γ -Fe₂O₃ is somewhat red shifted relative to the bulk due to surface effects.⁶⁶

The weak absorption corresponding to the EPT in γ -Fe₂O₃ implies a weak oscillator strength for this transition relative to the stronger electronic absorption transitions of γ -Fe₂O₃ at the UV end of the spectrum. Pershan and co-workers previously pointed out that the strength of dipole-forbidden crystal field transitions can be enhanced when electric-dipole transitions that can be ad-mixed to relieve the parity constraint lie close by in energy.^{42,67} The excitation of localized surface plasmons in our nanostructure provides strong dipoles spectrally and spatially close to the EPT. These plasmon resonances could lead to an increase in the transition strength of the EPT, allowing this transition to contribute to the magneto-optical response. Tomita et al. recently suggested the enhancement via strong near-field excitation of dipole-forbidden crystal field transitions in yttrium–iron garnet (YIG) thin films incorporating gold nanoparticles, to explain observed anomalies in the measured Kerr rotation spectrum in the region of the localized surface plasmon resonance.⁴² In combination with the enhancement of the EPT via intense electric fields, the likely presence of strong field gradients in the plasmonic field can relieve the parity constraint on these transitions.

In an equivalent picture, the composite magnetic/plasmonic nanostructure can be visualized to be a magnetic particle embedded in a resonant optical cavity. Because of the large density of photon states in the cavity, the interaction between the electromagnetic field of the light and the electronic transitions of the magnetic material is enhanced, resulting in a large Faraday rotation in this spectral region.

The magnitude of the magneto-optical enhancement is governed primarily by the spectral overlap of the magneto-optical transition and the plasmon resonance. The EPT is spectrally close to the plasmon resonance band at ~ 560 nm and is therefore enhanced and manifested as a well-resolved peak in the Faraday rotation spectrum. Another factor that contributes to the magnitude of the enhancement is the quality (energy/line-width) of the plasmon resonance mode. Narrow intense resonances are expected to provide the strongest enhancement. We observed significant Faraday rotation enhancement only from the nanoparticle sample (from Figure 2) with the most blue-shifted and narrow plasmon resonance.

In summary, we observed enhanced optical Faraday rotation, peaking at about 530 nm, in a composite plasmonic/magnetic nanostructure, consisting of gold-coated γ -Fe₂O₃ (maghemite) nanoparticles, whereas enhanced Faraday rotation was not observed in either uncoated γ -Fe₂O₃ nanoparticles or solid gold nanoparticles. The 530 nm Faraday rotation peak corresponds to an intrinsic electronic transition in the maghemite nanoparticles consistent with a surface plasmon resonance-enhanced magneto-optical (SuPREMO) effect. A more detailed theoretical understanding of the SuPREMO effect will be pursued in future work. Relevant parameters may include the following: magneto-optically active electronic transition matrix elements and their sensitivity to applied magnetic field; spectral and spatial overlap of the localized surface plasmon resonance with electronic transitions; and coupling between the plasmon resonance and magneto-optically active transitions. For future applications of the SuPREMO effect, it is advantageous that the spectrum of localized surface plasmon modes can be tuned by varying either the geometry or the choice of the plasmonic metal (e.g., gold, silver, copper).^{2,3,5,6,54} Colloidal techniques^{3,5,68} as well as nanolithography methods^{69–71} are well developed to achieve such tunability. Composite plasmonic/magnetic nanostructures are therefore a promising modality for enhanced and tailored optical polarization rotation, extended spectral range, and nanosized dimension. Such materials are desired in various applications including optical data storage, design of miniaturized magneto-optic devices, and optical sensing and imaging of magnetic fields and magnetic domain structures.^{29,72} An avenue for future research is to explore SuPREMO effects in other magneto-optical electronic transitions, including other ferrites³⁰ or Fe-containing garnets.^{29,58}

Acknowledgment. This work was supported partially by Siemens Healthcare and the Materials Research Science and Engineering Center of the National Science Foundation under NSF Award Number DMR-02-13805. We acknowledge the use of TEM facilities at the Center for Nanoscale Systems (CNS), a part of the Faculty of Arts and Sciences at Harvard

University and a member of the National Nanotechnology Infrastructure Network (NNIN), which is supported by the National Science Foundation under award no. ECS-0335765. We thank Dr. William Croft for XRD training and Dr. Darrick Chang for helpful discussions.

References

- (1) Bohren, C. F.; Huffman, D. R. *Absorption and Scattering of Light by Small Particles*; Wiley: New York, 1983.
- (2) Kelly, K. L.; Coronado, E.; Zhao, L. L.; Schatz, G. C. *J. Phys. Chem. B* **2003**, *107*, 668–677.
- (3) Halas, N. J. *MRS Bull.* **2005**, *30*, 362–367.
- (4) Mie, G. *Ann. Phys.* **1908**, *25*, 377–445.
- (5) Link, S.; El-Sayed, M. A. *Int. Rev. Phys. Chem.* **2000**, *19*, 409–453.
- (6) Jain, P. K.; Huang, X.; El-Sayed, I. H.; El-Sayed, M. A. *Acc. Chem. Res.* **2008**, *41*, 1578–1586.
- (7) El-Sayed, I. H.; Huang, X.; El-Sayed, M. A. *Nano Lett.* **2005**, *5*, 829–834.
- (8) Loo, C., A.; Lowery, A.; Halas, N.; West, J.; Drezek, R. *Nano Lett.* **2005**, *5*, 709–711.
- (9) Haes, A. J.; Van Duyne, R. P. *J. Am. Chem. Soc.* **2002**, *124*, 10596–10604.
- (10) Elghanian, R.; Storhoff, J. J.; Mucic, R. C.; Letsinger, R. L.; Mirkin, C. A. *Science* **1997**, *277*, 1078–1080.
- (11) Sonnichsen, C.; Reinhard, B. M.; Liphardt, J.; Alivisatos, A. P. *Nat. Biotechnol.* **2005**, *23*, 741–745.
- (12) Hirsch, L. R.; Stafford, R. J.; Bankson, J. A.; Sershen, S. R.; Rivera, B.; Price, R. E.; Hazle, J. D.; Halas, N. J.; West, J. L. *Proc. Natl. Acad. Sci. U.S.A.* **2003**, *100*, 13549–13554.
- (13) Huang, X.; El-Sayed, I. H.; Qian, W.; El-Sayed, M. A. *J. Am. Chem. Soc.* **2006**, *128*, 2115–2120.
- (14) Hao, E.; Schatz, G. C. *J. Chem. Phys.* **2004**, *120*, 357–366.
- (15) Sweatlock, L. A.; Maier, S. A.; Atwater, H. A.; Penninkhof, J. J.; Polman, A. *Phys. Rev. B* **2005**, *71*, 235408.
- (16) Schuck, P. J.; Fromm, D. P.; E., W.; Sundaramurthy, A.; Kino, G. *Phys. Rev. Lett.* **2005**, *94*, 017402.
- (17) Anderson, M. S. *Appl. Phys. Lett.* **2008**, *92*, 123101–123103.
- (18) Schatz, G. C.; Van Duyne, R. P. Electromagnetic Mechanism of Surface-enhanced Spectroscopy. In *Handbook of Vibrational Spectroscopy*; Chalmers, J. M., Griffiths, P. R., Eds.; Wiley: New York, 2002; pp 759–774.
- (19) Schatz, G. C. *Acc. Chem. Res.* **1984**, *17*, 370–376.
- (20) Nie, S.; Emory, S. R. *Science* **1997**, *275*, 1102–1106.
- (21) Jiang, J.; Bosnick, K.; Maillard, M.; Brus, L. *J. Phys. Chem. B* **2003**, *107*, 9964–9972.
- (22) Aslan, K.; Lakowicz, J. R.; Szmajkowski, H.; Geddes, C. D. *J. Fluoresc.* **2004**, *14*, 677–679.
- (23) Boyd, G. T.; Yu, Z. H.; Shen, Y. R. *Phys. Rev. B* **1986**, *33*, 7923–7936.
- (24) Tam, F.; Goodrich, G. P.; Johnson, B. R.; Halas, N. J. *Nano Lett.* **2007**, *7*, 496–501.
- (25) Stockman, M. I.; Bergman, D. J.; Anceau, C.; Brasselet, S.; Zyss, J. *Phys. Rev. Lett.* **2004**, *92*, 057402.
- (26) Chen, K.; Durak, C.; Heflin, J. R.; Robinson, H. D. *Nano Lett.* **2007**, *7*, 254–258.
- (27) Kim, S.; Jin, J.; Kim, Y.; Park, I.; Kim, Y.; Kim, S. *Nature* **2008**, *453*, 757–760.
- (28) Sundaramurthy, A.; Schuck, P. J.; Conley, N. R.; Fromm, D. P.; Kino, G. S.; Moerner, W. E. *Nano Lett.* **2006**, *6*, 355–360.
- (29) Scott, G. B.; Lacklison, D. E. *IEEE Trans. Magn.* **1976**, 292–311.
- (30) Scott, G. B.; Lacklison, D. E.; Ralph, H. I.; Page, J. L. *Phys. Rev. B* **1975**, *12*, 2562–2571.
- (31) Volkenstein, M. V.; Sharonov, J. A.; Shemelin, A. K. *Nature* **1966**, *209*, 709–710.
- (32) Andlauer, B.; Schneider, J.; Wettling, W. *Appl. Phys. A* **1976**, *10*, 189–201.
- (33) Diwekar, M.; Kamaev, V.; Shi, J.; Vardeny, Z. V. *Appl. Phys. Lett.* **2004**, *84*, 3112–3114.
- (34) Kahl, S.; Grishin, A. M. *Appl. Phys. Lett.* **2004**, *84*, 1438–1440.
- (35) Khanikaev, A. B.; Baryshev, A. V.; Fedyanin, A. A.; Granovsky, A. B.; Inoue, M. *Opt. Express* **2007**, *15*, 6612–6622.
- (36) Belotelov, V. I.; Doskolovich, L. L.; Zvezdin, A. K. *Phys. Rev. Lett.* **2007**, *98*, 077401.
- (37) Armeltes, G.; González-Díaz, J. B.; García-Martín, A.; García-Martín, J. M.; Cebollada, A.; González, M. U.; Acimovic, S.; Cesario, J.; Quidant, R.; Badenes, G. *Opt. Express* **2008**, *16*, 16104–16112.

- (38) Fujikawa, R.; Baryshev, A. V.; Kim, J.; Uchida, H.; Inoue, M. *J. Appl. Phys.* **2008**, *103*, 07D301.
- (39) Gonzalez-Diaz, J. B.; Garcia-Martin, A.; Garcia-Martin, J. M.; Cebollada, A.; Armelles, G.; Sepulveda, B.; Alaverdyan, Y.; Kall, M. *Small* **2008**, *4*, 202–205.
- (40) Hui, P. M.; Stroud, D. *Appl. Phys. Lett.* **1987**, *50*, 950–952.
- (41) Shemer, G.; Markovich, G. *J. Phys. Chem. B* **2002**, *106*, 9195–9197.
- (42) Tomita, S.; Kato, T.; Tsunashima, S.; Iwata, S.; Fujii, M.; Hayashi, S. *Phys. Rev. Lett.* **2006**, *96*, 167402.
- (43) Smith, D. A.; Stokes, K. L. *Opt. Express* **2006**, *14*, 5746–5754.
- (44) Abe, M.; Suwa, T. *Phys. Rev. B* **2004**, *70*, 235103.
- (45) Li, Y.; Zhang, Q.; Nurmikko, A. V.; Sun, S. *Nano Lett.* **2005**, *5*, 1689–1692.
- (46) Katayama, T.; Suzuki, Y.; Awano, H.; Nishihara, Y.; Koshizuka, N. *Phys. Rev. Lett.* **1988**, *60*, 1426–1429.
- (47) Feil, H.; Haas, C. *Phys. Rev. Lett.* **1987**, *58*, 65–68.
- (48) Safarov, V. I.; Kosobukin, V. A.; Hermann, C.; Lampel, G.; Peretti, J.; Marlière, C. *Phys. Rev. Lett.* **1994**, *73*, 3584–3587.
- (49) Bonod, N.; Reinisch, R.; Popov, E.; Nevière, M. *J. Opt. Soc. Am. B* **2004**, *21*, 791–797.
- (50) Bennett, W. R.; Schwarzacher, W.; Egelhoff, W. F. *Phys. Rev. Lett.* **1990**, *65*, 3169.
- (51) Lyon, J. L.; Fleming, D. A.; Stone, M. B.; Schiffer, P.; Williams, M. E. *Nano Lett.* **2004**, *4*, 719–723.
- (52) Cornell, R. M.; Schwertmann, U. *The Iron Oxides: Structure, Properties, Reactions, Occurrences, and Uses*; Wiley-VCH: New York, 1996.
- (53) Brown, K. R.; Natan, M. J. *Langmuir* **1998**, *14*, 726–728.
- (54) Oldenburg, S. J.; Averitt, R. D.; Westcott, S. L.; Halas, N. J. *Chem. Phys. Lett.* **1998**, *288*, 243–247.
- (55) Jain, P. K.; El-Sayed, M. A. *Nano Lett.* **2007**, *7*, 2854–2858.
- (56) Slack, F. G. *Phys. Rev.* **1934**, *46*, 945–947.
- (57) Jain, A.; Kumar, J.; Zhou, F.; Li, L.; Tripathy, S. *Am. J. Phys.* **1999**, *67*, 714–717.
- (58) Wittekoek, S.; Popma, T. J. A.; Robertson, J. M.; Bongers, P. F. *Phys. Rev. B* **1975**, *12*, 2777.
- (59) Sherman, D. M.; Burns, R. G.; Mee Burns, V. J. *Geophys. Res.* **1982**, *87*, 10169–10180.
- (60) Sherman, D. M.; Waite, T. D. *Am. Mineral.* **1985**, *70*, 1262–1269.
- (61) Tang, J.; Myers, M.; Bosnick, K. A.; Brus, L. E. *J. Phys. Chem. B* **2003**, *107*, 7501–7506.
- (62) Cabot, A.; Puentes, V. F.; Shevchenko, E.; Yin, Y.; Balcells, L.; Marcus, M. A.; Hughes, S. M.; Alivisatos, A. P. *J. Am. Chem. Soc.* **2007**, *129*, 10358–10360.
- (63) Bajt, S.; Sutton, S. R.; Delaney, J. S. *Geochim. Cosmochim. Acta* **1994**, *58*, 5209–5214.
- (64) Litter, M. I.; Blesa, M. A. *Can. J. Chem.* **1992**, *70*, 2502–2510.
- (65) Chakrabarti, S.; D.; Ganguli, D.; Chaudhuri, S. *Physica E* **2004**, *24*, 333–342.
- (66) Ziolo, R. F.; Giannelis, E. P.; Weinstein, B. A.; O'Horo, M. P.; Ganguly, B. N.; Mehrotra, V.; Russell, M. W.; Huffman, D. R. *Science* **1992**, *257*, 219–223.
- (67) Kahn, F. J.; Pershan, P. S.; Remeika, J. P. *Phys. Rev. Lett.* **1968**, *21*, 804–807.
- (68) Jana, N. R.; Gearheart, L.; Murphy, C. J. *Adv. Mater.* **2001**, *13*, 1389–1393.
- (69) Fromm, D. P.; Sundaramurthy, A.; Schuck, P. J.; Kino, G.; Moerner, W. E. *Nano Lett.* **2004**, *4*, 957–961.
- (70) Jain, P. K.; Huang, W.; El-Sayed, M. A. *Nano Lett.* **2007**, *7*, 2080–2088.
- (71) Hulteen, J. C.; Treichel, D. A.; Smith, M. T.; Duval, M. L.; Jensen, T. R.; Van Duyne, R. P. *J. Phys. Chem. B* **1999**, *103*, 3854–3863.
- (72) Zayat, M. Z.; del Monte, F.; Morlaes, M. D.; Rosa, G.; Guerrero, H.; Serna, C. J.; Levy, D. *Adv. Mater.* **2003**, *15*, 1809–1812.

NL900007K